PtCu Single-Atom Alloys as coke-resistant catalysts for efficient C-H activation

Matthew D. Marcinkowski[1‖], Matthew T. Darby[2‖], Jilei Liu[3‖], Joshua M. Wimble[3], Felicia R. Lucci[1], Sungsik Lee[4], Angelos Michaelides[5], Maria Flytzani-Stephanopoulos[3], Michail Stamatakis[2]* and E. Charles H. Sykes[1]**

1. Department of Chemistry, Tufts University, 62 Talbot Avenue, Medford, Massachusetts 02155, United States.
2. Thomas Young Centre and Department of Chemical Engineering, University College London, Roberts Building, Torrington Place, London WC1E 7JE, United Kingdom
3. Department of Chemical and Biological Engineering, Tufts University, 4 Colby Street, Medford, Massachusetts 02155, United States
4. X-ray Science Division, Argonne National Laboratory, 9700 S. Cass Avenue, Argonne, Illinois 60439, United States.
5. Thomas Young Centre, London Centre for Nanotechnology and Department of Physics and Astronomy, University College London, Gower Street, London WC1E6BT, United Kingdom

‖ denotes authors contributed equally to the work

**Corresponding author*

maria.flytzani-stephanopoulos@tufts.edu

m.stamatakis@ucl.ac.uk

charles.sykes@tufts.edu

Abstract

The recent availability of shale gas has led to a renewed interest in C-H bond activation as the first step towards synthesis of fuels and fine chemicals. Heterogeneous catalysts based on Ni and Pt can perform this chemistry, but deactivate easily due to coke formation. Cu- based catalysts are not practical for this chemistry due to high C-H activation barriers, but their weaker binding to adsorbates offers resilience to coking. Utilizing Pt/Cu single atom alloys (SAAs) we examine C-H activation in a number of systems including methyl groups, methane, and butane using a combination of simulations, surface science, and catalysis studies. We find that Pt/Cu SAAs activate C-H bonds more efficiently than Cu, are stable for days under realistic operating conditions, and avoid the problem of coking typically encountered with Pt. Pt/Cu SAAs therefore offer a new approach to coke resistant C-H activation chemistry with the added economic benefit that the precious metal is diluted at the atomic limit.

The production of shale gas from hydraulic fracturing has boosted the supply of light alkanes such as ethane and propane in recent years.[1,2] However, there are few low-carbon footprint methods that efficiently convert these gases to more valuable chemicals due to their relative inertness.[3] While steam cracking is the traditional industrial process, it is energy-demanding and less than 60% efficient.[2] Catalytic processes are sought after to improve the energy balance sheet. Facile activation of C-H bonds in alkanes would open new routes to synthesize commodity and fine chemicals.[3–6] There are numerous ways to functionalize alkanes including alkane halogenation/oxyhalogenation, oxidative coupling, and oxidative dehydrogenation.[7–10] This study will focus on the dehydrogenation of alkanes to produce alkenes, which are precursors to industrially relevant polymers.[1,6,11,12] Ni catalysts are often used for C-H activation, as Ni is inexpensive, but these suffer from coking since Ni breaks C-C bonds in alkanes and can completely dehydrogenate alkanes to carbon.[13,14] Preventing coking is indeed an active, yet challenging area of current research.[15] Pt catalysts also suffer from coking and Pt's high price prohibits widespread use.[16–18] Cu catalysts are typically not considered viable due to a high C-H activation barrier on Cu surfaces, but are resistant to coking.[19]

Alloys often exhibit unique properties compared to their constituent metals.[20,21] For example, using a combination of surface science, theory, and high surface area catalysis Besenbacher et al. showed that small amounts of Au dispersed in Ni can suppress carbon deposition in methane steam reforming by both raising the barrier to C-H activation and decreasing the binding strength of carbon to the surface.[20] We take the opposite approach, using the smallest amount of a catalytic metal (Pt) in the form of single atoms in the surface layer of a more inert host metal (Cu) to facilitate C-H activation while avoiding coking that typically occurs on larger ensembles.[21] These *single atom alloys* (SAAs)[22–24] are analogous to single atom catalysts[25,26], but unlike many single atom catalysts, reaction at the active site can be understood with atomistic detail on SAAs. Using a combination of simulations and surface science, we probe the reaction mechanism of C-H activation on these alloy surfaces and find that

PtCu alloys activate C-H bonds with significantly improved activity over Cu, while avoiding coking that occurs on catalysts with extended Pt ensembles due to Cu's ability to facilitate C-C coupling chemistry. These PtCu alloy nanoparticle catalysts exhibit reaction temperatures significantly lower than Cu under realistic operating conditions. We provide unique insight into the atomic scale structure of the catalytically active sites, spillover of intermediates, and the thermodynamics and kinetics of the reaction pathway. The PtCu nanoparticle catalysts we have developed via this approach show great promise for the C-H chemistries and illustrate the paradigm of coupling surface science with catalysis as a promising direction for catalyst development.

Results and Discussion

Model Catalysts Studies

To understand C-H activation in a well-defined system, we study single crystals under ultra-high vacuum (UHV) conditions which allows the surface reactivity and selectivity measured with temperature programmed reaction (TPR) to be related to the atomic scale structure of the active sites and the reaction intermediates imaged with high-resolution scanning tunnelling microscopy (STM). The alloying mechanism of Pt into Cu was previously characterized and representative STM images are shown in Figure 1a-b.[22–24] In these alloys Pt atoms are able to alloy both directly into the terraces and in regions near the step edges and are randomly distributed throughout the surface. By controlling the temperature during alloying we ensure that Pt atoms remain predominately in the surface layer and are mono-dispersed. Using density functional theory (DFT) we calculate the adsorption energy of CH_x fragments and the activation energies for the various possible C-H bond scission elementary events on Pt(111), Cu(111) and Pt/Cu(111) SAAs. Moreover, we incorporate the DFT data into kinetic Monte Carlo (KMC) simulations of TPR, which are essential for interpreting the experimental results and explaining the unique surface chemistry of Pt/Cu SAAs.

TPR Experiments

Methyl iodide (CH_3I) provides a simple method for adding methyl groups to our alloy surfaces and TPR studies of subsequent methane evolution allows us to examine C-H activation energetics. CH_3I has been well studied on a number of metal surfaces in UHV, including Pt and Cu, and is known to dissociate to form CH_3 and I at low temperature.[18,27–33] At low coverage, the main effect of iodine is as a site blocker and the C-H activation temperature is relatively unaffected across a range of iodine coverages (Supplementary Figures 1 and 2).[33,34] TPR spectra resulting from the reaction of 4.5 Langmuirs (1 L = 1 X 10^{-6} Torr·s) of CH_3I on pure Cu, a 0.01 monolayer (ML) Pt/Cu(111) SAA, and 1 ML Pt/Cu(111) are presented in Figure 1c. The major desorption product for each surface is methane. Ethene, ethane, and propene are also produced (Supplementary Figure 3). Desorption of intact CH_3I is not detected at these exposures. For clarity, only traces for methane and ethene are displayed in Figure 1b. Desorption of these products is reaction rate limited as small hydrocarbons normally desorb from Cu(111) at very low temperatures.[30,35,36] The black spectra correspond to the reaction of CH_3I on Cu(111) and agree well with previously published results on this surface.[30,31] Methane and the larger hydrocarbons desorb at ~450 K. It has been previously demonstrated that the rate limiting step to form these products is the activation of C-H bonds in methyl groups to produce methylene and H_a.[27,28] Methane is formed by facile hydrogenation of remaining methyl groups, while the coupling of methylene and methyl forms larger hydrocarbons. These C-C coupling reactions allow Cu(111) to avoid coking.[30,31] The red spectra in Figure 1c correspond to CH_3I on a 0.01 ML Pt/Cu(111) SAA alloy. On the SAA surface, methane and carbon coupling products desorb at ~350 K, *100 K cooler than on the pure Cu(111) surface*. Because the rate limiting step in methane evolution is C-H activation, this 100 K temperature shift reveals that single Pt atoms in the Cu surface significantly lower the barrier to C-H activation in CH_3. The formation of ethene, ethane and propene implies the Pt/Cu SAA maintains the ability of Cu to avoid coking via C-C coupling. Experiments adding deuterium to the surfaces verified that C-H activation was still the rate limiting step

on the SAA (Supplementary Figure 4)[22,23,32,37] The blue spectra in Figure 1c correspond to the reaction of CH_3I on a surface where 1 ML of Pt has been deposited on Cu(111) (Supplementary Figure 5). The majority of methane desorbs at ~250 K, a temperature close to that of methyl decomposition on a Pt(111) crystal.[18,32] Despite activating C-H bonds at a low temperature, on Pt(111) methylene groups do not couple and eventually decompose to surface bound carbon and gas phase H_2.[18,29,32] No coupling products are observed at 250 K on the 1 ML Pt/Cu(111) surface, showing that this alloy is more similar to Pt(111) than Cu(111). Hydrogen from methylene decomposition desorbs at high temperature similar to Pt(111) (Supplementary Figure 6).[18,32] No hydrogen desorbs from Cu(111) or the Pt/Cu(111) SAA surfaces, confirming their resistance to coking. Examining alloy surface composition, intermediate to 0.01 ML and 1 ML Pt, reveals generally that as the amount of Pt increases the temperature of C-H activation drops, but so does the production of coupling products (Supplementary Figure 7).

Computational Studies

To further understand and support our experimental data, we evaluate the kinetics of methane dehydrogenation on Cu(111), Pt/Cu(111) SAA and Pt(111) using KMC simulations (Figure 1d). Simulated TPR spectra of species from a methyl covered lattice are used to study the rate of methane desorption as a function of temperature. KMC is used to analyze and identify the elementary processes contributing to the observed methane desorption rate and determine the typical reaction temperatures for successive scissions of C-H bonds in methane-derived species on each surface. To parameterize a KMC simulation, we generate a list of elementary events with associated rate constants. For calculating the latter we employ the Eyring equation within the framework of transition state theory (TST), with activation energies and pre-exponentials computed from first principles (see Supplementary section A.8).

We use DFT to study the successive scission of C-H bonds from methane through to atomic carbon. First, we find the most stable configurations for all C_xH_y species (x=0,1; y=0, 1,2,3,4) on the Cu(111), Pt/Cu(111) SAA and Pt(111) surfaces. Three adsorption sites are considered for each adsorbate on each surface, namely atop, bridge and hollow. The formation energies (E_F) of the most stable configurations with the corresponding site type for each species on each surface are given in Table 3 in the Supplementary Information. DFT structures of the most stable configurations on Pt/Cu(111) SAA are shown in Figure 2a; the corresponding configurations for Cu(111) and Pt(111) are shown in Figure 10 in the Supplementary Information.

Transition states for C-H bond scission steps from CH_4* to C* on each of the three surfaces, were computed using the dimer method and are verified with vibrational frequency analysis.[38,39] The corresponding activation energies are given in Table 4 of the Supplementary information. The DFT structures for the transition states of each C-H bond scission on the Pt/Cu(111) SAA are shown in Figure 2b. We note clear differences in the energetics of each pathway despite the comparable intermediate and transition state molecular geometries we have computed. Figure 2c elucidates why Pt(111) is an active C-H activation catalyst, exhibiting much lower barriers for all C-H scissions considered when compared to Cu(111). However, the strong binding of CH_x intermediates to the Pt(111) surface compared to Cu(111) explains the tendency for coke to form on Pt C-H activation catalysts and the lack thereof on Cu. Interestingly, the Pt/Cu(111) SAA exhibits intermediate barrier heights compared to the two pure metals. Dehydrogenations of CH_x species on Pt/Cu(111) SAA and Cu(111) are endothermic, however the net pathway on Pt(111) is exothermic. These findings explain our experimental observations that the Pt/Cu(111) SAA may readily activate C-H bonds in adsorbed CH_3* while resisting coke formation.

TPR Simulations

Using KMC simulations, we analyse the reliability of our DFT calculations and provide further insight into the kinetics and reaction pathways that give rise to the experimental observations previously discussed, ascertaining the temperatures and extent of each activation. We simulate TPR using KMC on Cu(111), Pt/Cu(111) SAA and Pt(111). In each simulation, the lattice was randomly initialized with CH_3* only and the temperature ramped from 160 K to 560 K at a heating rate of 1 K/s. Extensive details on the simulation setup are found in Supplementary section A.7. By initializing each surface with H (in addition to methyl), rapid hydrogenation of methyl to methane occurs at around 200 K (Supplementary Figure 4). In the absence of such pre-dosed H, CH_3* must first dehydrogenate in order to detect any subsequent methane desorption. Therefore, the C-H scission of CH_3* is rate limiting for methane production, and the temperature at which this occurs is surface dependent. We simulate methane TPR peak temperatures of 451 K, 373 K and 288 K for Cu(111), Pt/Cu(111) SAA and Pt(111) respectively (Figure 1d). Each TPR profile agrees well with the experimental data, strongly supporting the reliability of our DFT calculations.

On Cu(111) and the Pt/Cu(111) SAA, further dehydrogenations of CH* to carbon are not observed within the simulated temperature range, though these do occur on Pt(111) as a result of a lower barrier and the exothermic nature of the overall pathway (Figure 2c, blue curves). The facile formation of CH* and C* at low temperature on Pt(111) likely prevents the coupling of CH* and CH_2 fragments to form C_2H_x or C_3H_y species that are observed experimentally as desorption products from the Pt/Cu(111) SAA. Inevitably this leads to coking of the Pt(111) surface through the production of carbon-rich species.

STM Experiments

We performed STM experiments to examine reaction intermediates not detectable in the TPR experiments and to confirm that no coke is formed on the Pt/Cu SAA surface. Figure 3a-h shows a series of images taken after annealing the system to progressively higher temperatures for both Cu(111) and 0.01 ML Pt/Cu(111). After an 80 K anneal, below the temperature necessary for C-I bond cleavage, intact CH_3I appears in the images as disordered clusters on both surfaces (Figure 3a and b). Annealing either surface to 120 K results in new ordered structures (Figure 3c and d). On both surfaces there are intermixed bright and dark features arranged in large well-defined 2D clusters forming a $\sqrt{3}x\sqrt{3}\ R30°$ structure. A high-resolution STM image clearly displaying this structure is shown in Figure 3i. The clusters exhibit similar behaviour to pure methyl groups formed via pyrolysis of azomethane on Cu(111).[41] The bright features are iodine atoms while the darker features are CH_3. For the Pt/Cu surface shown in Figure 3d, some individual iodine atoms are separated from clusters, marking positions where iodine is absorbed on Pt atoms. Annealing to higher temperatures between 350-450 K causes notable changes in the adsorbate structures on Cu(111) vs. 0.01 ML Pt/Cu(111) (Figure 3e and f). On Cu(111) both bright and dark features are on the surface, while on Pt/Cu(111) only bright features remain in a $\sqrt{3}x\sqrt{3}\ R30°$ structure (Figure 3j). This is consistent with the TPR results which reveal that on 0.01 ML Pt/Cu(111), C-H activation of CH_3 occurs at 350 K followed by immediate desorption of methane and coupling products. Figure 3f shows that after annealing to 350 K, the Pt/Cu(111) SAA surface contains only patches of iodine atoms which appear as bright protrusions in a $\sqrt{3}x\sqrt{3}\ R30°$ structure, in agreement with previous reports.[33,41–43] However, annealing the Cu(111) surface to 350 K is insufficient to activate C-H bonds and so methyl groups are still observed in Figure 3e; while for Pt/Cu(111) in Figure 3f, the C-H bond has been activated leaving only adsorbed iodine atoms.[43] Importantly, no other species besides iodine are observed on the Pt/Cu(111) surface, indicating it does not suffer from coking by carbon like pure Pt(111). Annealing the Cu(111) surface further to 450 K (Figure 3g) allows for C-H bond

activation, hydrocarbon desorption, leaving only iodine on the surface. On the Pt/Cu(111) surface no change is observed after annealing to 450 K (Figure 3h). Iodine is very stable on Cu(111) and desorbs above 800 K.[43] Annealing either surface above 1000 K results in a clean Cu(111) surface (Supplementary Figure 15), further demonstrating that no carbon remains.

Ambient pressure C-H activation studies

Encouraged by the results in our model studies, we studied C-H activation with PtCu SAAs under ambient pressure catalytic reaction conditions. Butane-deuterium isotope scrambling (B-D scrambling) experiments were performed with nanoparticle (NP) catalysts in a flow reactor. The production rate of deuterated butane in B-D scrambling experiments indicates the C-H activation capability of the catalysts as hydrogen (deuterium) dissociation is a facile process under the reaction conditions applied.[23,37] The reaction was operated within the kinetics controlled regime (conversion < 5%), so that the effluent concentration of B-D scrambling products is proportional to the overall C-H activation rate.

$Pt_{0.03}$Cu-SAA and $Pt_{0.01}$Cu-SAA NPs were prepared by a galvanic replacement reaction as reported in Lucci et al. and Liu et al.[23,37] (see Supplementary Table 5 and section B.2) and supported on silica. Extended X-Ray absorption fine structure (EXAFS) and Fourier transform infrared spectroscopy (FTIR) results confirm the formation of NPs with isolated Pt atoms (Supplementary Figures 16-21 and Table 6).

We compared the performance of Cu NPs and PtCu SAA NP catalysts for B-D scrambling using temperature programmed surface reaction (TPSR) (Figure 4a). $Pt_{0.03}$Cu-SAA and $Pt_{0.01}$Cu-SAA start to convert butane (C_4H_{10}) to deuterated butane (C_4H_9D) at around 250 °C but the Cu-NP is active only at temperatures above 500 °C (Supplementary Figure 22). This demonstrates that the activity of B-D scrambling i.e. C-H activation, is significantly improved by the addition of a small amount of Pt into the Cu surface. Figure 4b shows that Pt-NPs begin to catalyse the B-D scrambling around 100 °C. Thus, TPSR

suggests the barriers of C-H activation on the NP catalysts follow the order: Pt < PtCu-SAA < Cu. This corroborates the trend of C-H activation barriers identified in the model catalyst studies.

Pure Pt NP catalysts rapidly deactivate during the reaction (Figure 4b). In the first cycle of TPSR, the production of C_4H_9D 'lights-off' at 100 °C and increases with increasing temperature up to 230 °C. The production rate of C_4H_9D then drops off after 230 °C indicating significant deactivation, overcoming the effect of temperature increase on reaction rate. The second and third cycles of TPSR show much lower activity compared to the first cycle and the activity decreases cycle by cycle. On the other hand, PtCu-SAAs are very stable. Figure 4c shows that $Pt_{0.01}Cu$-SAA catalyses the B-D scrambling at 360 °C without any deactivation for at least 12 hours. CO-FTIR of the spent catalyst indicates that the Pt atoms remain isolated in PtCu SAA NPs post reaction (Supplementary Figures 18 and 19). These results demonstrate the structural stability of PtCu SAA NPs under atmospheric pressure reaction conditions.

Our surface science studies showed that extended Pt surfaces can over-dehydrogenate methyl groups and cause carbon deposition. To verify this coking in the NP catalysts we performed temperature-programmed-oxidation (TPO) on used catalysts to determine whether carbon deposition occurs during B-D scrambling. Pt-NP and $Pt_{0.01}Cu$-SAA were both exposed to B-D scrambling conditions at 360 °C for 12 hours prior to TPO measurements. As shown in Figure 5, a broad CO_2 evolution from the used Pt-NP is seen, beginning at 130 °C. At least two different types of carbon are shown, the second matching graphitic carbon oxidation[44], while any adsorbed hydrocarbon species must have desorbed during the Ar heat treatment. These features are absent on the $Pt_{0.01}Cu$-SAA. The amount of CO_2 produced from this catalyst is essentially the same as that produced from the silica support without any hydrocarbon exposure. Thus, PtCu SAAs are coke- resistant at atmospheric pressure reaction conditions while Pt NPs catalyse carbon formation and deposition, which causes severe deactivation of the catalyst during the B-D scrambling conditions.

To investigate the coke resistance of PtCu SAAs under realistic catalytic reaction conditions, we conducted the non-oxidative dehydrogenation of butane to butene over $Pt_{0.01}Cu$-SAA. We found the reactivity was stable for at least 52 hours at 400 °C (Supplementary Figure 25) and only minimal carbon deposition on $Pt_{0.01}Cu$-SAA compared to Pt-NP (Supplementary Figure 26).

Conclusion

C-H activation was examined on PtCu SAAs using a combination of single crystal studies in UHV, simulations, and supported nanoparticle catalyst tests in a flow reactor at atmospheric pressure. Our TPR and STM results reveal that SAAs activate C-H bonds in methyl groups at 350 K, 100 K cooler than Cu, while avoiding the coke formation observed on Pt surfaces. We rationalize these results with DFT studies that examine a succession of C-H scissions in methane. Our calculations show that compared to the pure metals, SAAs have intermediate barriers for C-H activation and the formation of dehydrogenated fragments is endothermic, therefore the Pt/Cu(111) SAA surface is active but does not coke. In addition, KMC simulations using the activation barriers and binding energies calculated from DFT agree very well with our TPR study. Our catalytic studies with supported PtCu, Pt, and Cu NPs show that PtCu-SAAs activate C-H bonds using the B-D scrambling reaction in butane. We find that the PtCu SAAs catalyse the exchange reaction at 250 °C compared to ~550 °C on Cu NPs and are stable during the reaction. Pt NPs activate the reaction at temperatures as low as 100 °C, but quickly deactivate due to coking. These findings, taken collectively with the surface science studies and simulations, illustrate that PtCu SAAs are promising catalysts for C-H bond activation in small alkane molecules at moderate temperatures, and can be further developed as robust catalysts resistant to coking that plagues traditional Pt, Pd and Ni catalysts. Furthermore, our study highlights an example of translating the results of theoretical and single crystal studies to the design of practical catalysts, which to date, is an approach rarely reported in the literature[20]. However, with recent innovations in simulation, imaging

techniques, and catalyst synthesis/characterisation we expect that this approach will become more commonplace.

Methods

UHV Experiments

Experiments were performed in two different UHV chambers. The first UHV chamber with a base pressure of 1×10^{-10} mbar incorporated a quadrupole mass spectrometer (Hiden) for performing TPR experiments. A heating rate of 1 K/s was used for our TPR experiments. M/z 142 was monitored to detect CH_3I. M/z 41, 30, and 27 were monitored for propene, ethane, and ethene respectively. M/z 16 and 15 were monitored for methane. M/z 28 was monitored for various hydrocarbon fragments and for CO. M/z 18 and 2 were monitored for water and hydrogen. Per surface science convention TPR results are reported in K. The sample was held at 80 K during gas exposures. The second UHV chamber was an Omicron Nanotechnology LT-UHV STM with a base pressure < $1x10^{-11}$ mbar. STM images were obtained at 5 K. The instrument also incorporates a separate chamber for sample preparation. Clean Cu(111) (99.9999% Princeton Scientific) was prepared via Ar^+ sputtering followed by annealing to 750 K in the TPR chamber and 1000 K in the STM chambers. This treatment results in a step density of ~1%. Liquid CH_3I (Sigma Aldrich 99.5%) was degassed through freeze-pump thaw cycles before being introduced into the chambers. Hydrogen 99.999% and deuterium 99.999% were purchased from AirGas. Molecules were dosed on the Cu(111) crystals by backfilling the chamber to a desired pressure for a certain time using high precision leak valves. Exposures were calculated in Langmuirs (1 L = $1x10^{-6}$ torr·s). Pt deposition was accomplished using flux-monitored Omicron Nanotechnology Focus EFM 3 electron beam evaporators. Pt coverages were calibrated using CO (Airgas, 99.99%) adsorption.

Computational Details

Periodic density functional theory calculations were performed using the Vienna *ab initio* Simulation Package (VASP) version 5.4.1.[45,46] The exchange-correlation functional used is the non-local OptB86b-vdW functional,[47] which is a revised version of the van der Waals density functional of Dion et al.[48] We use a 3 × 3 × 5 slab unit cell whereby the top-most four layers are allowed to fully relax while the bottom-most layer is fixed at the OptB86b-vdW bulk FCC lattice constant (Cu = 3.608 Å, Pt = 3.958 Å) and a vacuum length of 10 Å separates periodic images in the z-direction. For surface calculations on Pt/Cu(111) SAA we use the lattice constant of FCC Cu and replace a single atom of Cu in the surface layer of the Cu(111) slab with a Pt atom. The Brillouin zone is sampled by a 13 × 13 × 1 Monkhorst-Pack k-point mesh and the planewave kinetic energy cutoff is set to 400 eV (see Supplementary section A.9). We ensure electronic self-consistency up to a tolerance of $<10^{-7}$ eV and the Hellmann-Feynman forces on free atoms during ionic relaxation are optimized to be $<10^{-2}$ eV·Å^{-1}. We present formation energies (E_F) of surface species with respect to gas phase CH_4 and H_2, which we take as references (having formation energies equal to zero). For a given surface species C_xH_y $x = \{0,1\}, y = \{0,1,2,3,4\}$, we write the formation energy ($E_F(C_xH_y)$) as

$$E_F(C_xH_y) = E_{tot}(C_xH_y + slab) - \left\{E_{tot}(slab) + x \cdot E_{tot}(CH_4) - \left(\frac{4x-y}{2}\right) \cdot E_{tot}(H_2)\right\} \quad (1)$$

We write the activation energy (E_a) as the DFT total energy of the transition state ($E_{Tot}^{\ddagger}$) minus the DFT total energy of the initial state (E_F^{IS}):

$$E_a = E_{Tot}^{\ddagger} - E_{Tot}^{IS} \quad (2)$$

We perform simulations within the graph-theoretical KMC framework as implemented in Zacros version 1.02.[49,50] The simulation temperature is ramped from 160 K to 560 K at a rate of 1 K·s^{-1} to mimic

TPR. The partial pressures of gas phase species (CH_4 and H_2) are set to zero in order to reproduce ultra-high vacuum conditions. The simulation cell is formed of (30 × 31) fcc unit cells with periodic boundary conditions. Simulations for the Pt/Cu(111) SAA make use of a lattice whereby Cu sites have been randomly substituted with Pt sites giving a Pt density of 0.039; this is slightly higher that the overall Pt concentration in experiment in order to reflect a higher density of Pt atoms closer to step edges. The surface is randomly initialized with 0.25 ML coverage of methyl and wherever noted 0.25 ML of hydrogen adatoms.

Nanoparticle Studies

Synthesis and Characterization: PtCu NP catalysts were prepared as previously described.[23,37,51] Copper NPs prepared as colloids by reducing $Cu(NO_3)_2$ in aqueous solution with $NaBH_4$ as reducing agent and polyvinylpyrrolidone as capping agent. The resulting copper NPs were deposited onto a silica support (fumed silica, 0.2-0.3 μm average aggregate particle size, surface area 200 m^2/g) followed by calcination in air at 300 °C.[23,37,52] $Pt_{0.03}$Cu-SAA and $Pt_{0.01}$Cu-SAA were prepared by the galvanic replacement method on the copper NPs.[23,37] Experimental and analysis details on the XAS, CO-IR and other characterizations for the NPs catalysts are discussed in the Supplementary section B.

Catalytic activity measurements: B-D scrambling experiments were performed in a packed-bed flow microreactor (L=22 inch, O.D.=1/2 inch) with 100 mg of catalyst diluted by 1 g of quartz particles. Per convention we present our catalytic results in °C. Prior to the introduction of reaction gas mixture (5% Butane, 2% Deuterium and balance Argon), the samples were reduced in 20% H_2/He at 400 °C for 20 minutes and cooled to ambient temperature. After stabilizing in the reaction gas mixture at ambient temperature for 1 hour, the temperature was raised to the desired point. The gas effluent from the reactor was analyzed by a mass-spectrometer. To perform temperature programmed B-D scrambling, the temperature was increased from ambient temperature to 400 °C at 5 °C/min.

Data availability: Additional methods and materials characterization can be found in Supplementary Information. All data supporting the findings of this study are available upon request from the corresponding authors.

References

1. Sattler, J. J. H. B., Ruiz-Martinez, J., Santillan-Jimenez, E. & Weckhuysen, B. M. Catalytic dehydrogenation of light alkanes on metals and metal oxides. *Chem. Rev.* **114,** 10613–10653 (2014).
2. Alper, J. *The Changing Landscape of Hydrocarbon Feedstocks for Chemical Production: Implications for Catalysis: Proceedings of a Workshop*. (The National Academies Press, 2016).
3. Shilov, A. E. & Shul'pin, G. B. Activation of C-H bonds by metal complexes. *Chem. Rev.* **97,** 2879–2932 (1997).
4. Labinger, J. A. & Bercaw, J. E. Understanding and exploiting C-H bond activation. *Nature* **417,** 507–514 (2002).
5. Wencel-Delord, J. & Glorius, F. C–H bond activation enables the rapid construction and late-stage diversification of functional molecules. *Nat. Chem.* **5,** 369–375 (2013).
6. Zhao, Z.-J., Chiu, C. & Gong, J. Molecular understandings on heterogeneous catalytic dehydrogenation of light alkanes. *Chem. Sci.* **6,** 4403–4425 (2015).
7. Lin, R., Amrute, A. P. & Pérez-Ramírez, J. Halogen-mediated conversion of hydrocarbons to commodities. *Chem. Rev.* **117,** 4182–4247 (2017).
8. McFarland, E. Unconventional chemistry for unconventional natural gas. *Science* **338,** 340–342 (2012).
9. Gärtner, C. A., van Veen, A. C. & Lercher, J. A. Oxidative dehydrogenation of ethane: common principles and mechanistic aspects. *ChemCatChem* **5,** 3196–3217 (2013).
10. Schwarz, H. Chemistry with methane: concepts rather than recipes. *Angew. Chemie - Int. Ed.* **50,** 10096–10115 (2011).
11. Guo, X. *et al.* Direct, Nonoxidative Conversion of Methane to Ethylene, Aromatics, and Hydrogen. *Science* **344,** 616–620 (2014).
12. Schweitzer, N. M. *et al.* Propylene Hydrogenation and Propane Dehydrogenation by a Single-Site Zn 2 + on Silica Catalyst. *ACS Catal.* **4,** 1091–1098 (2014).
13. Swaan, H. M., Kroll, V. C. H., Martin, G. A. & Mirodatos, C. Deactivation of supported nickel catalysts during the reforming of methane by carbon dioxide. *Catal. Today* **21,** 571–578 (1994).
14. Ruckenstein, E. & Hu, Y. H. Carbon dioxide reforming of methane over nickel/alkaline earth metal oxide catalysts. *Appl. Catal. A* **133,** 149–161 (1995).
15. Taccardi, N. *et al.* Gallium-rich Pd-Ga phases as supported liquid metal catalysts. *Nat. Chem.* 1–6 (2017). doi:10.1038/nchem.2822
16. Jiang, F. *et al.* Propane Dehydrogenation over Pt/TiO2-Al2O3 Catalyst. *ACS Catal.* **5,** 438–447

(2015).

17. Iglesias-Juez, A. *et al.* A combined in situ time-resolved UV-Vis, Raman and high-energy resolution X-ray absorption spectroscopy study on the deactivation behavior of Pt and PtSn propane dehydrogenation catalysts under industrial reaction conditions. *J. Catal.* **276,** 268–279 (2010).
18. Henderson, M. A., Mitchell, G. E. & White, J. M. The chemisorption of methyl halides (Cl, Br, and I) on Pt(111). *Surf. Sci.* **184,** L325–L331 (1987).
19. Yang, F., Koeller, J. & Ackermann, L. Photoinduced copper-catalyzed C-H arylation at room temperature. *Angew. Chem. Int. Ed.* **55,** 4759–4762 (2016).
20. Besenbacher, F. *et al.* Design of a surface alloy catalyst for steam reforming. *Science* **279,** 1913–1915 (1998).
21. Rodriguez, J. A. Physical and chemical properties of bimetallic surfaces. *Surf. Sci. Rep.* **24,** 223–287 (1996).
22. Lucci, F. R., Marcinkowski, M. D., Lawton, T. J. & Sykes, E. C. H. H2 activation and spillover on catalytically relevant Pt–Cu single atom alloys. *J. Phys. Chem. C* **119,** 24351–24357 (2015).
23. Lucci, F. R. *et al.* Selective hydrogenation of 1,3-butadiene on platinum–copper alloys at the single-atom limit. *Nat. Commun.* **6,** 8550 (2015).
24. Lucci, F. R., Lawton, T. J., Pronschinske, A. & Sykes, E. C. H. Atomic scale surface structure of Pt/Cu(111) surface alloys. *J. Phys. Chem C.* **118,** 3015–3022 (2014).
25. Yang, X. F. *et al.* Single-atom catalysts: a new frontier in heterogeneous catalysis. *Acc. Chem. Res.* **46,** 1740–1748 (2013).
26. Thomas, J. M., Saghi, Z. & Gai, P. L. Can a single atom serve as the active site in some heterogeneous catalysts? *Top. Catal.* **54,** 588–594 (2011).
27. Azizian, S. & Gobal, F. Mechanism of catalytic decomposition of CH3I on the Cu(111) surface: a UBI-QEP approach. *Langmuir* **16,** 8095–8099 (2000).
28. Chiang, C.-M., Wentzlaff, T. H. & Bent, B. E. Iodomethane decomposition on Cu(110): surface reactions of C1 fragments. *J. Phys. Chem.* **96,** 1836–1848 (1992).
29. French, C. & Harrison, I. Orientation and decomposition kinetics of methyl iodide on Pt(111). *Surf. Sci.* **342,** 85–100 (1995).
30. Lin, J.-L. & Bent, B. E. Iodomethane dissociation on Cu(111): Bonding and chemistry of adsorbed methyl groups. *J. Vac. Sci. Technol. A* **10,** 2202–2209 (1992).
31. Lin, J.-L. & Bent, B. E. Two mechanisms for formation of methyl radicals during the thermal decomposition of CH3I on a Cu(111) surface. *J. Phys. Chem.* **97,** 9713–9718 (1993).
32. Zaera, F. Study of the surface chemistry of methyl iodide coadsorbed with hydrogen on Pt(111). *Surf. Sci.* **262,** 335–350 (1992).
33. Pascal, M. *et al.* Methyl on Cu(111)— structural determination including influence of co-adsorbed iodine. *Surf. Sci.* **512,** 173–184 (2002).
34. Chao-Ming, C. & Bent, B. E. Methyl radical adsorption on Cu(111): Bonding, reactivity, and the effect of coadsorbed iodine. *Surf. Sci.* **279,** 79–88 (1992).
35. Canning, N. D. S., Baker, M. D. & Chesters, M. A. Ethylene and acetylene adsorption on Cu(111) and Pt(111) studied by Auger spectroscopy. *Surf. Sci.* **111,** 441–451 (1981).

36. Meyers, J. M. & Gellman, A. J. The investigation of fluorinated propenes on the Cu(111) surface. *Surf. Sci.* **339,** 57–67 (1995).

37. Liu, J. *et al.* Tackling CO Poisoning with single atom alloy catalysts. *J. Am. Chem. Soc.* **138,** 6396–6399 (2016).

38. Henkelman, G. & Jónsson, H. A dimer method for finding saddle points on high dimensional potential surfaces using only first derivatives. *J. Chem. Phys.* **111,** 7010–7022 (1999).

39. Henkelman, G. & Jónsson, H. Improved tangent estimate in the nudged elastic band method for finding minimum energy paths and saddle points. *J. Chem. Phys.* **113,** 9978–9985 (2000).

40. Psofogiannakis, G., St-Amant, A. & Ternan, M. Methane oxidation mechanism on Pt(111): a cluster model DFT study. *J. Phys. Chem. B* **110,** 24593–24605 (2006).

41. Chan, Y. L., Pai, W. W. & Chuang, T. J. Direct observation of methyl radicals islanding on copper surfaces and its effects on the kinetics of catalytic reactions. *J. Phys. Chem. B* **108,** 815–818 (2004).

42. Michaelides, A. & Hu, P. Softened C-H modes of adsorbed methyl and their implications for dehydrogenation: An ab initio study. *J. Chem. Phys.* **114,** 2523–2526 (2001).

43. Andryushechkin, B. V., Eltsov, K. N. & Shevlyuga, V. M. Atomic scale observation of iodine layer compression on Cu(111). *Surf. Sci.* **472,** 80–88 (2001).

44. Deng, W. & Flytzani-Stephanopoulos, M. On the Issue of the Deactivation of Au–Ceria and Pt–Ceria Water–Gas Shift Catalysts in Practical Fuel-Cell Applications. *Angew. Chemie* **118,** 2343–2347 (2006).

45. Kresse, G. & Furthmüller, J. Efficiency of ab-initio total energy calculations for metals and semiconductors using a plane-wave basis set. *Comput. Mater. Sci.* **6,** 15–50 (1996).

46. Kresse, G. & Furthmüller, J. Efficient iterative schemes for ab initio total-energy calculations using a plane-wave basis set. *Phys. Rev. B* **54,** 11169–11186 (1996).

47. Klimeš, J., Bowler, D. R. & Michaelides, A. Van der Waals density functionals applied to solids. *Phys. Rev. B - Condens. Matter Mater. Phys.* **83,** 195131 (2011).

48. Dion, M., Rydberg, H., Schröder, E., Langreth, D. C. & Lundqvist, B. I. Van der Waals density functional for general geometries. *Phys. Rev. Lett.* **92,** 246401 (2004).

49. Stamatakis, M. & Vlachos, D. G. A graph-theoretical kinetic Monte Carlo framework for on-lattice chemical kinetics. *J. Chem. Phys.* **134,** 214115 (2011).

50. Nielsen, J., D'Avezac, M., Hetherington, J. & Stamatakis, M. Parallel kinetic Monte Carlo simulation framework incorporating accurate models of adsorbate lateral interactions. *J. Chem. Phys.* **139,** 224706 (2013).

51. Marcinkowski, M. D. *et al.* Selective formic acid dehydrogenation on Pt-Cu single atom alloys. *ACS Catal.* **7,** 413–420 (2017).

52. Boucher, M. B. *et al.* Single atom alloy surface analogs in Pd0.18Cu15 nanoparticles for selective hydrogenation reactions. *Phys. Chem. Chem. Phys.* **15,** 12187–12196 (2013).

Acknowledgements

All surface science studies (M.D.M., F.R.L., E.C.H.S.) were performed with support from the Division of Chemical Sciences, Office of Basic Energy Sciences, CPIMS Program, U.S. Department of Energy, under Grant No. FG02-10ER16170. J.L. and M.F-S. thank the U.S. Department of Energy (DE-FG02-05ER15730) for the financial support of the catalysis work. The XAS research used resources of the Advanced Photon Source, a U.S. Department of Energy Office of Science, User Facility operated for the Department of Energy Office of Science by Argonne National Laboratory under Contract No. DE-AC02-06CH11357. M.T.D is funded by the Engineering and Physical Sciences Research Council UK as part of a Doctoral Training Grant. The authors acknowledge the use of the UCL High Performance Computing Facilities (Legion@UCL and Grace@UCL), and associated support services, in the completion of the computational part of this work. The theoretical portion of the research also used resources of the Oak Ridge Leadership Computing Facility, which is a DOE Office of Science User Facility supported under Contract DE-AC05-00OR22725. Access to the Oak Ridge facility was provided via the Integrated Mesoscale Architectures for Sustainable Catalysis (IMASC), an Energy Frontier Research Center funded by the U.S. Department of Energy, Office of Science, Basic Energy Sciences under Award #DE-SC0012573. A.M. is supported by the European Research Council under the European Union's Seventh Framework Programme (FP/2007-2013)-European Research Council Grant agreement no. 616121 (HeteroIce project). A.M. is also supported by the Royal Society through a Royal Society Wolfson Research Merit Award.

Author contributions

M.D.M. performed the TPR experiments. M.T.D. performed the DFT and KMC calculations. M.D.M. and F.R.L. performed the STM experiments. J.L. and J.W. performed the nanoparticle experiments. S.L.

performed the EXAFS measurements. M.D.M., M.T.D. and J.L. analysed the data from their relevant experimental contributions. M.D.M., M.T.D., J.L., A.M., M.F-S., M.S. and E.C.H.S. wrote the manuscript. All authors read and commented on the manuscript.

Additional information

Supplementary information is available in the online version of the paper. Reprints and permissions information is available online at www.nature.com/reprints. Correspondence for materials should be addressed to M.F-S., M.S. and E.C.H.S.

Competing financial interests

The authors declare no competing financial interests.

Figure Captions

Figure 1. Methane evolution as a reporter of C-H activation in methyl groups on various surface structures; experiment and simulation. (a) STM image of a 0.01 ML Pt/Cu(111) SAA surface. Scale bar = 1.5 nm. (b) Wide-scale image of the 0.01 monolayer (ML) Pt/Cu(111) SAA surface showing that Pt is distributed across both terraces and at regions near step edges. Scale bar = 1 nm. Inset shows an atomic resolution image of the alloy surface. Scale bar = 0.5 nm. (c) TPR traces taken with a heating rate of 1 $K \cdot s^{-1}$ showing the evolution of methane (solid lines) and ethene (dashed lines) from Cu(111) (black), 0.01 ML Pt/Cu(111) (red) and 1.0 ML Pt/Cu(111) (blue) surfaces following deposition of 4.5 L of CH_3I. (d) Simulated TPR of methyl covered Cu(111) (black), Pt/Cu(111) SAA (red) and Pt(111) (blue). The simulation randomly initializes the surface with 0.25 ML CH_3 at 160 K and ramps the temperature at a rate of 1 $K \cdot s^{-1}$ for 400 s to a final temperature of 560 K. The normalized TPR signal is plotted as the derivative of the number of gas phase molecules of methane evolved from the surface with respect to time. The experiments and theory show that the Pt/Cu SAA activates C-H bonds at significantly lower temperature than Cu while also avoiding coking seen on extended Pt surfaces.

Figure 2. Comparison of the reaction pathways between pure and SAA surfaces shows that Pt/Cu(111) SAAs have intermediate C-H scission barriers but beneficial Cu-like reaction energies, such that the SAA can perform C-H activation without carbon deposition. Optimized configurations from density functional theory are shown for a) the most stable adsorptions of C_xH_y species (x=0,1; y=0, 1,2,3,4) on the Pt/Cu(111) SAA surface; and b) the transition states (TS) for C-H bond scissions from CH_4* to CH_3* + H* (TS1), CH_3* to CH_2* + H* (TS2), CH_2* to CH* + H* (TS3) and CH* to C* + H* (TS4) on the Pt/Cu(111) SAA surface. An energy landscape for the full dehydrogenation of adsorbed CH_4* on Cu(111) (black), Pt/Cu(111) SAA (red) and Pt(111) (blue) is given in c).

Figure 3. STM imaging of reaction intermediates on Cu(111) and Pt/Cu SAA surfaces revealing lower temperature C-H activation on Pt/Cu SAAs than Cu. (a-h) STM images at 5 K show the various stages of the reaction of CH_3I on Cu(111) and 0.01 ML Pt/Cu(111) surfaces (top and bottom rows respectively) after annealing to various temperatures. Scale bars = 3 nm. Panels a and b show clusters of intact MeI molecules. In panels (c-h) dissociated iodine atoms appears as higher, brighter protrusions, while methyl groups appear as darker protrusions. (i) High resolution STM images of mixed phase methyl (darker protrusions) and iodine (brighter protrusions) after a 120 K anneal on Cu(111) and (j) iodine on Cu(111) after a 450 K anneal. Scale bars = 1 nm for (i) and (j). These STM images confirm what was predicted by the TPR results, namely that the Pt/Cu SAA surface is able to activate C-H bonds in methyl groups at lower temperature than Cu while still avoiding carbon deposition.

Figure 4. Reactor studies of butane-deuterium scrambling as a reporter of C-H activation and long term catalyst stability of NP catalysts. TPSR data for the B-D scrambling reaction over (a) $Pt_{0.03}$Cu-SAA, $Pt_{0.01}$Cu-SAA and Cu-NP catalysts and (b) Pt-NP catalysts, monitored by mass spectrometry. (Temperature ramp 5°C/min) The 59/58 mass ratio indicates the C_4H_9D amount. The data in (a) are from the second reaction cycle. First, second and third cycles of TPSR are shown for Pt-NP (b); (c) 12-hour test for the $Pt_{0.01}$Cu-SAA catalyst at 360°C showing stability over time. The catalyst was at room temperature at the beginning and end of the test. Gas composition: 5% butane, 2% deuterium and balance argon. 50 ml/min, 100 mg catalysts. These flow reactor studies show PtCu SAA NPs catalyse C-H activation in butane molecules at lower temperature than Cu without the deactivation observed for Pt NPs.

Figure 5. Oxidation tests reveal a lack of coking of Pt/Cu SAA catalysts. Temperature programmed oxidation (TPO) of Pt-NP (blue), $Pt_{0.01}$Cu-SAA (red) and silica (green). Pt-NP and $Pt_{0.01}$Cu-SAA were treated in B-D scrambling reaction conditions at 360°C for 12 hours. All systems were treated in an argon flow at 300°C for 2 hours before TPO to desorb the hydrocarbon adsorbates. TPO conditions: 20% O_2/He, 20 mL/min, 3°C/min, 100 mg catalysts. TPO experiments confirm there is no carbon deposition on PtCu SAA NPs, only the silica, at ambient pressure reaction conditions while Pt NPs are subject to significant carbon deposition.

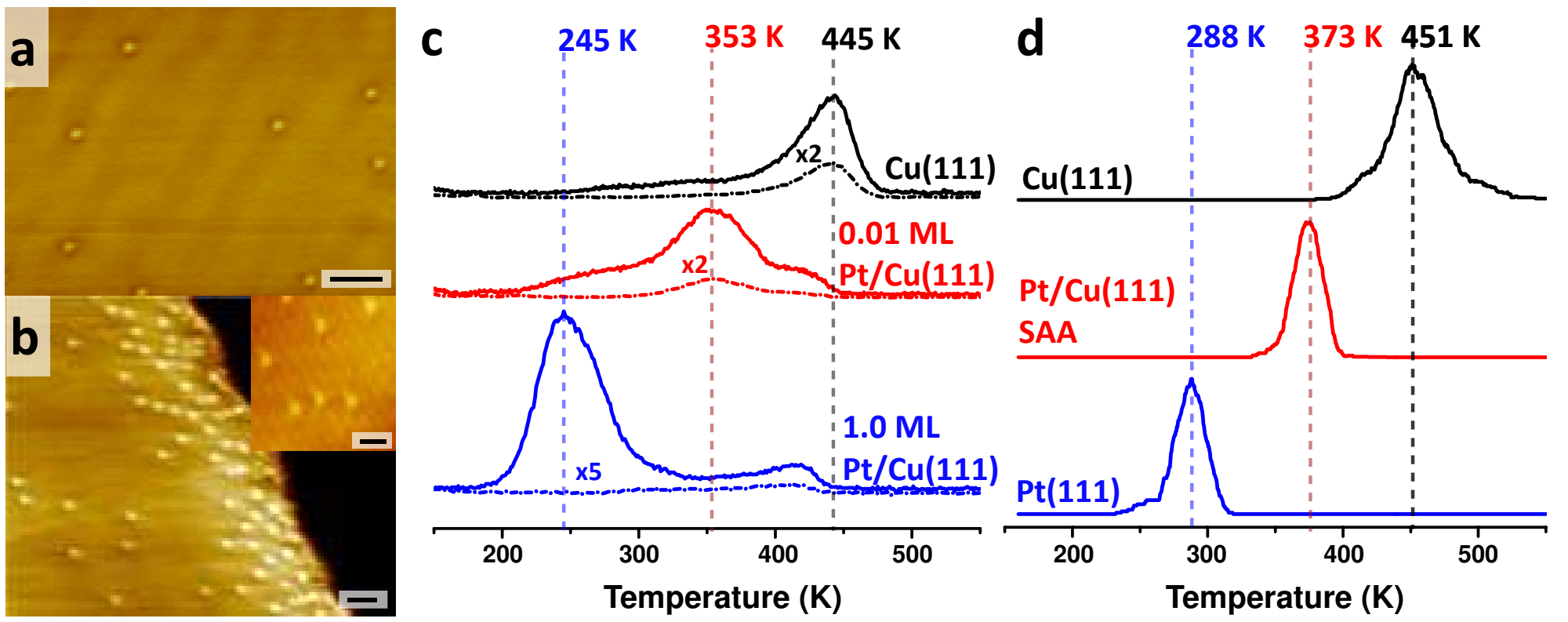
a
b
c
245 K
353 K
445 K
x2
Cu(111)
0.01 ML
Pt/Cu(111)
x2
1.0 ML
Pt/Cu(111)
x5
200
300
400
500
Temperature (K)
d
288 K
373 K
451 K
Cu(111)
Pt/Cu(111)
SAA
Pt(111)
200
300
400
500
Temperature (K)

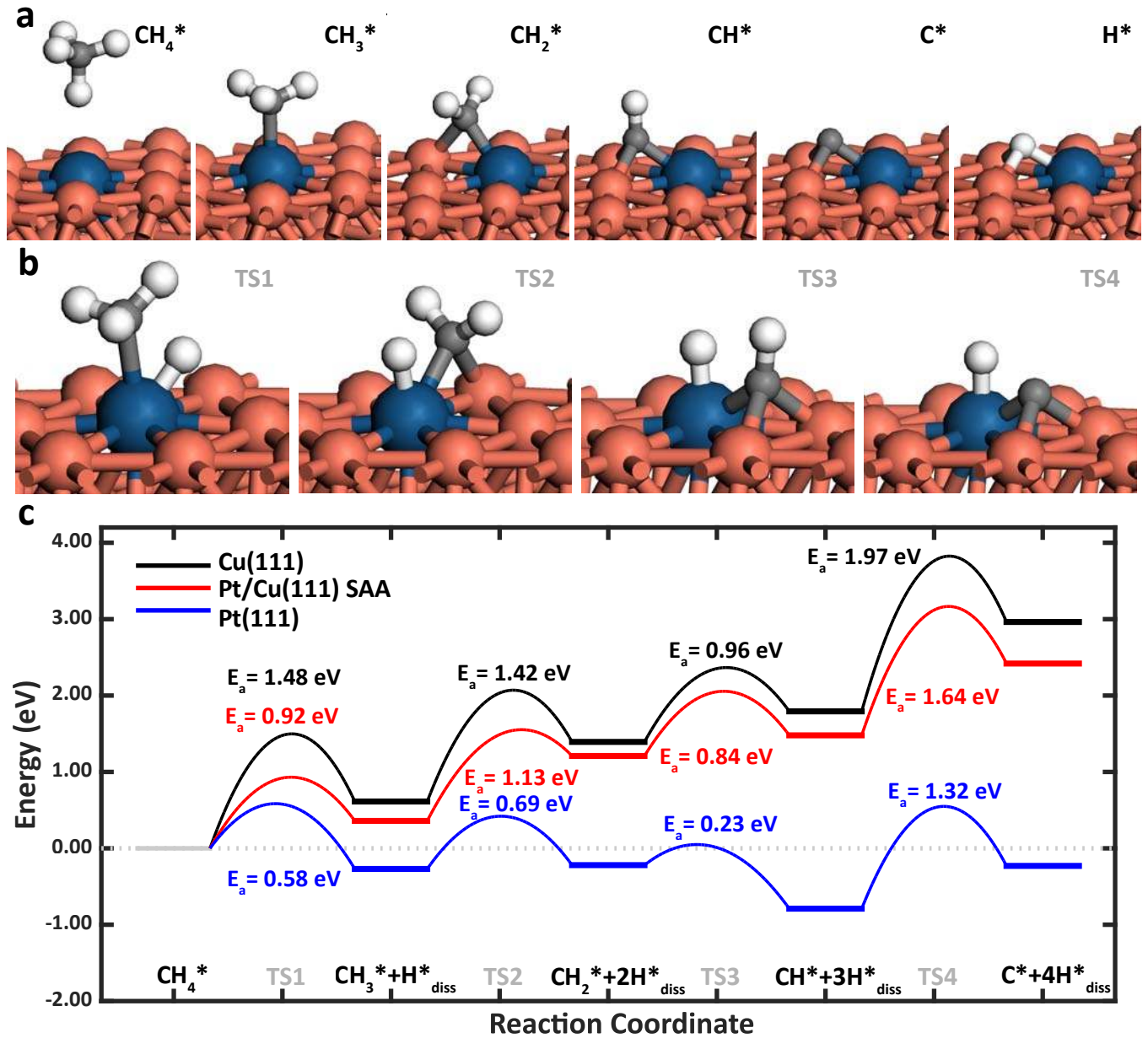
a
CH4*
CH3*
CH2*
CH*
C*
H*
b
TS1
TS2
TS3
TS4
c
Cu(111)
Pt/Cu(111) SAA
Pt(111)
Ea = 1.48 eV
Ea = 0.92 eV
Ea = 0.58 eV
Ea = 1.42 eV
Ea = 1.13 eV
Ea = 0.69 eV
Ea = 0.96 eV
Ea = 0.84 eV
Ea = 0.23 eV
Ea = 1.97 eV
Ea = 1.64 eV
Ea = 1.32 eV
Energy (eV)
4.00
3.00
2.00
1.00
0.00
-1.00
-2.00
CH4*
TS1
CH3*+H*diss
TS2
CH2*+2H*diss
TS3
CH*+3H*diss
TS4
C*+4H*diss
Reaction Coordinate

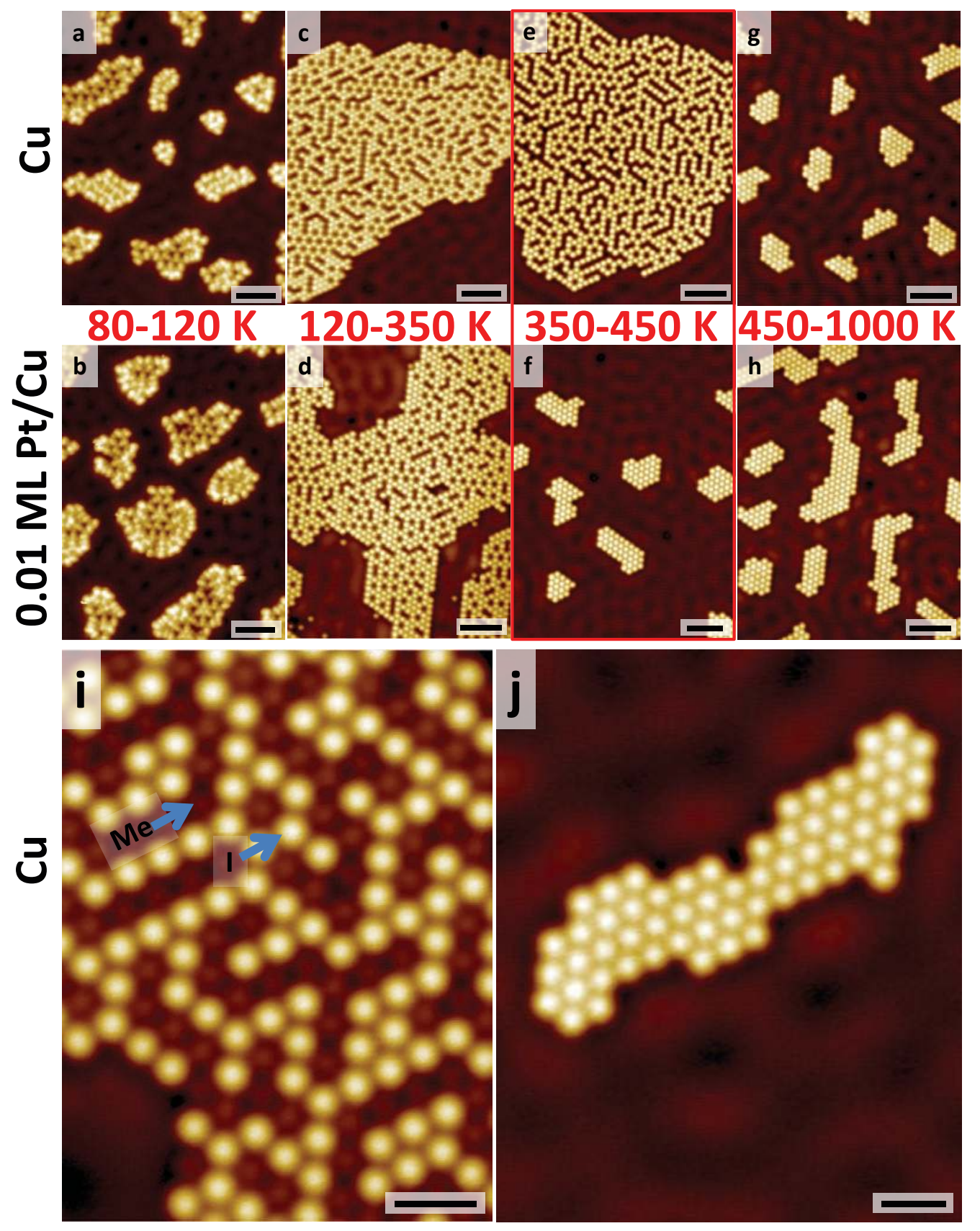
Cu
a
c
e
g
80-120 K
120-350 K
350-450 K
450-1000 K
0.01 ML Pt/Cu
b
d
f
h
Cu
i
Me
I
j

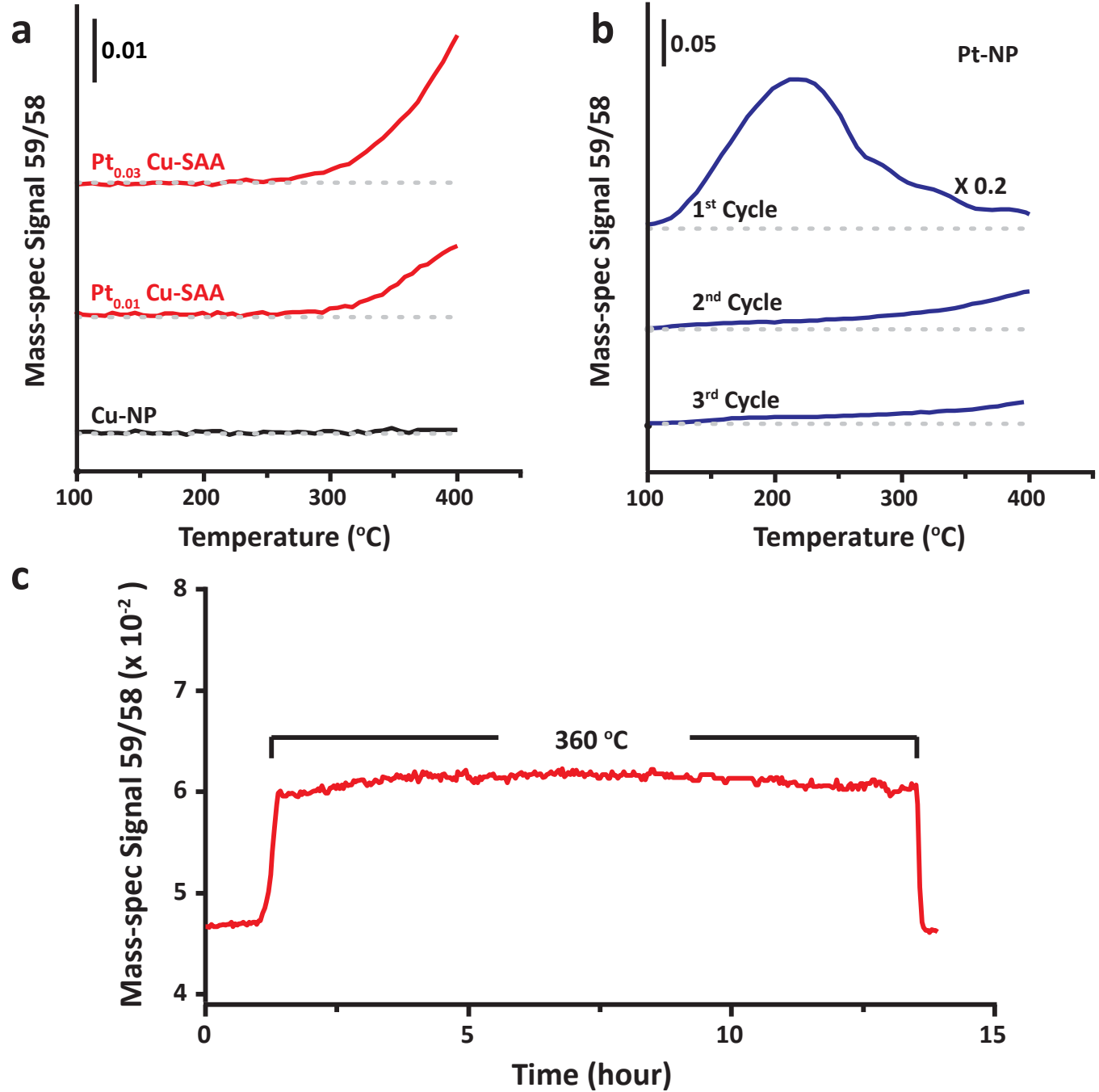
a
0.01
Pt0.03 Cu-SAA
Pt0.01 Cu-SAA
Cu-NP
Mass-spec Signal 59/58
100
200
300
400
Temperature (°C)
b
0.05
Pt-NP
X 0.2
1st Cycle
2nd Cycle
3rd Cycle
Mass-spec Signal 59/58
100
200
300
400
Temperature (°C)
c
360 °C
Mass-spec Signal 59/58 (x 10-2)
8
7
6
5
4
0
5
10
15
Time (hour)

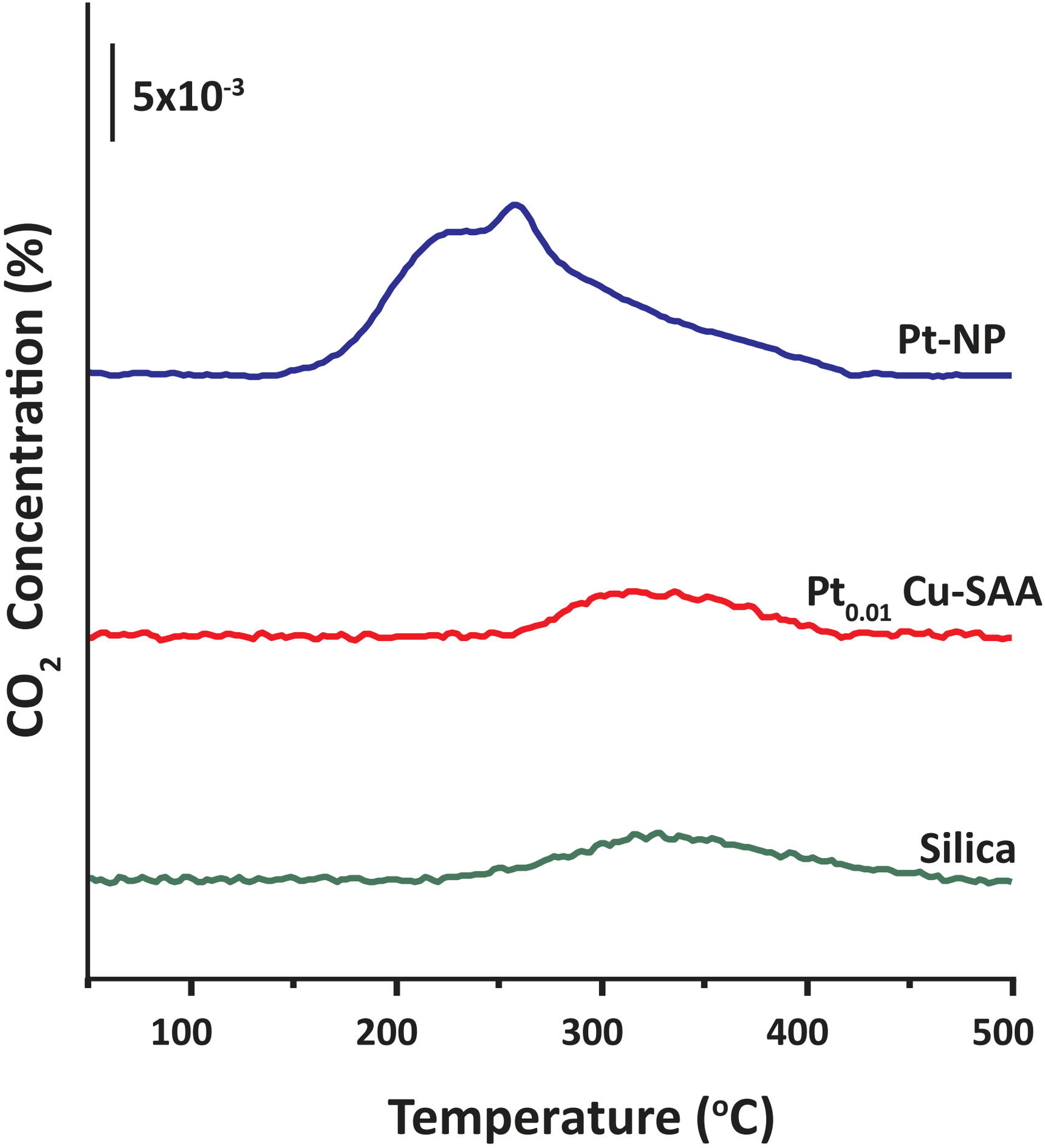
5x10-3
CO2 Concentration (%)
Pt-NP
Pt0.01 Cu-SAA
Silica
100
200
300
400
500
Temperature (°C)

C-H Activation on PtCu *Single Atom Alloys*

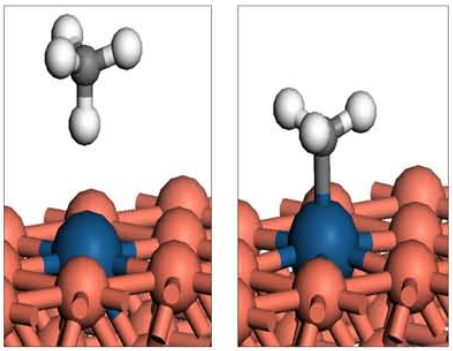

Theory
0 K, 0 Bar

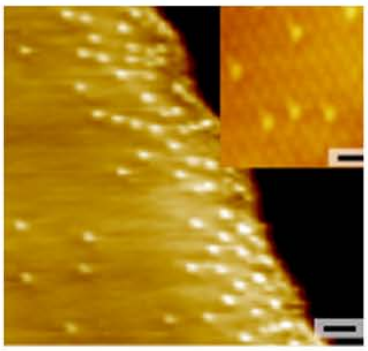

Model System
300 K, 10^{-13} Bar

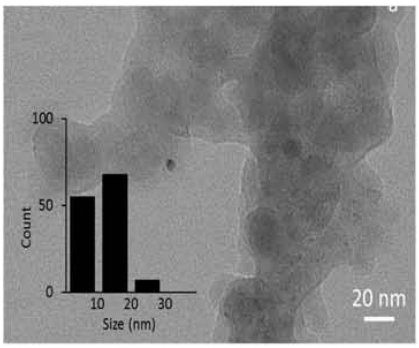

Catalyst
400°C, 1 Bar